AIAA 81-4090

Three-Dimensional Theory for the Steady Loading on an Annular Blade Row

Gregory F. Homicz* and John A. Lordi*
Calspan Corporation, Buffalo, N.Y.

A lifting-surface analysis is presented for the steady, three-dimensional, subsonic flow through an annular blade row. A kernel-function procedure is used to solve the linearized integral equation that relates the unknown blade loading to a specified camber line. The unknown loading is expanded in a finite series of prescribed loading functions, that allows the required integrations to be performed analytically. Numerical results are presented for a range of hub/tip ratios, solidities, and camber line geometries. As expected, two-dimensional strip theory shows good agreement with the present results for high hub/tip ratio, at least near midannulus. However, near the hub and tip, and particularly for low hub/tip ratios, the error introduced by the use of two-dimensional strip theory becomes significant. This is traced to the induced angle of attack generated by the trailing vortex wake, that is accounted for only in the three-dimensional theory. Comparisons are also made with the three-dimensional inverse (i.e., design) theory of Okurounmu and McCune. Their analysis yields the blade camber line required to produce a specified load distribution. By inputting their blade geometry to our program, we have been able to predict loadings in good agreement with those originally specified by them for two cases: one a free-vortex design, and another in which significant trailing vorticity is present.

Nomenclature

a	= sound speed
a_{ij}	= loading coefficients in expansion of $\Delta\hat{p}$, Eq. (12)
A_{mBk}, B_{mBk}	= defined in Eqs. (7a) and (7b)
B	= number of blades
$b_{n\ell}$	= camber line slope at (σ_n, x_ℓ)
c	= local blade chord (Fig. 2)
c_a	= axial projection of blade chord, a constant (Fig. 2)
$C^{\pm}, S^{\pm}$	= defined in Eq. (11b)
C^i	= axial integrals defined in Eq. (14a)
C^i_{mBk}	= axial cosine integrals defined in Eqs. (14b) and (14c)
h	= hub/tip ratio, r_H/r_T
$H(x)$	= Heaviside step function, $\frac{1}{2}[\mathrm{sgn}(x)+1]$
i,j	= indexes of chordwise and spanwise loading functions, respectively
I^j_{mBk}	= radial integrals defined in Eq. (13)
K_{mBk}	= radial eigenvalue
ℓ,n	= indexes of chordwise and spanwise collocation points, respectively
$L(\sigma)$	= sectional lift per unit span
L_θ	= tangential blade spacing, $2\pi r/B$
m,k	= azimuthal and radial duct mode indexes, respectively
M	= axial Mach number, $U/a_{-\infty}$
M_R	= relative Mach number, $U_R/a_{-\infty}$
NI,NJ,NK,NM	= term at which i,j,k and m series are truncated, respectively
NL,NN	= number of chordwise and spanwise collocation points, respectively
$\mathfrak{N}_{CL}$	= function describing the blade camber line
p	= perturbation pressure
$\hat{p}$	= nondimensional perturbation pressure, $p/\frac{1}{2}\rho_{-\infty}U^2$
r,θ,z	= cylindrical polar coordinates (Fig. 1)
R_{mBk}	= orthonormal radial eigenfunctions
s,n	= local streamwise and normal coordinates (Fig. 2)
$\hat{s}$	= nondimensional streamwise coordinate, Eq. (10)
$\mathrm{sgn}(x)$	= sign function, ± 1 for $x \gtrless 0$
S^i_{mBk}	= axial sine integrals defined in Eq. (14d)
U	= uniform axial velocity
U_R	= relative freestream velocity, $U\sqrt{1+(\omega r/U)^2}$
v	= perturbation velocity
V_{mBk}	= defined in Eq. (2c)
x	= nondimensional axial coordinate, Eq. (5b)
α_{3D}	= angle of attack relative to undisturbed helical inflow
β,β_R	= $(1-M^2)^{\frac{1}{2}}$ and $(1-M_R^2)^{\frac{1}{2}}$, respectively
$\hat{\Gamma}$	= nondimensional circulation, $\Gamma/(UL_{\theta T})$
ζ	= helical coordinate, $\theta-(\omega/U)z$
η_T	= $c_a/2r_T$
Λ_{mBk}	= defined in Eq. (2b)
λ_{mBk}	= defined in Eq. (2a)
ρ	= density
σ	= nondimensional radial coordinate, r/r_T
ϕ	= $\cos^{-1}x$
ϕ_T	= $\omega r_T/U$
ψ	= undisturbed flow angle, $\tan^{-1}(\omega r/U)$
ω	= rotor angular velocity

Subscripts

H	= evaluated at hub
T	= evaluated at tip
0	= source coordinate on surface, e.g., x_0, σ_0
$\pm\infty$	= conditions at $z=\pm\infty$

Superscript

$(\hat{\ })$	= dimensionless quantity

Received Feb. 11, 1980; revision received Oct. 6, 1980.

*Principal Engineer, Aerodynamic Research Dept., Advanced Technology Center. Member AIAA.

I. Introduction

As the tip speed of modern axial flow fans and compressors has entered the transonic regime, and the use of lower hub/tip ratios has increased, a need has developed for a better understanding of the three-dimensional effects that

occur in the blade rows of such machines. Fully numerical procedures are being applied to the solution of the three-dimensional equations of motion, but at present are still in the development stage. Moreover, they can be rather expensive in terms of computer time, particularly if a variety of off-design conditions must be considered.

The present paper seeks a solution to the fully three-dimensional, but linearized, steady flow equations. Although such an approach is in principle limited to low pressure ratios, it holds the promise of increasing our physical understanding of the rotor flowfield at a cost well below that of solving the fully nonlinear equations. The techniques developed subsequently should also prove useful in the solution of the unsteady loading case. This has application to the important problems of blade flutter, response to inlet distortion, and aerodynamic noise generation. For the time being, we consider only the steady subsonic case, and present a numerical collocation procedure for the solution of the linear integral equation relating the local loading on the blades of a rotating annular blade row to the upwash field at the blade surface.

The study of linearized, compressible three-dimensional flow through an annular blade row began with the early work of McCune, who initially considered only the disturbance generated by the blades' thickness distribution.[1-3] Okurounmu and McCune[4] extended the analysis to treat the loading problem wherein the circulation, $\Gamma(r)$, is specified a priori. Initially, they modeled each blade as a radially-oriented line vortex of variable spanwise strength, and were able to obtain useful expressions for the overall static and total pressure rise, and change in axial velocity. They later generalized this work to include finite chord effects in a lifting-surface type analysis, with the blades modeled as a distribution of horseshoe vortices.[5,6] Again, only the design problem was considered, i.e., computing the camber line required to produce a prescribed loading; this can be reduced to an integration over the known vortex distribution.

Just as in isolated airfoil theory, the solution to the off-design problem, in which one seeks the loading produced by blades with a prescribed camber line, is more difficult because it requires the inversion of an integral equation. McCune and Dharwadkar[7] considered this problem in the context of a Prandtl lifting-line approximation, using the type of analysis presented in Ref. 4. This work represented the extension to subsonic flow of Falcao's earlier investigation of the incompressible case.[8] Namba[9,10] was the first to treat the off-design problem using a lifting-surface type of analysis. He used pressure dipole singularities to represent the blade loading, in contrast to the vortex representation of McCune et al.[4-7] Salaun[11,12] later applied a pressure dipole representation to the prediction of the unsteady blade loading. Although not concerned with the steady problem per se, Salaun briefly discussed it in Appendix D of Ref. 12; however, no numerical results were obtained for this problem.

Thus, the present work, which also employs a pressure dipole approach, most closely parallels that of Namba; in fact, the basic flow model and the assumptions made are almost identical. However, the present analysis differs in two important respects from that of Refs. 9 and 10. The first is that the integral equation treated here is not the same as that solved by Namba, as will be seen later. In a companion paper by the present authors,[13] the linearized analysis leading to this equation is reviewed in detail, and it is concluded that the present form of the equation is the correct one. In addition, it is shown there both that the present formulation agrees with the form given by Salaun,[12] and that it is equivalent to that derived by Okurounmu and McCune[5,6] based on the horseshoe vortex representation, which further reinforces the preceding conclusion.

The present paper is primarily concerned with the numerical solution of the integral equation. This is the second feature distinguishing our treatment of this problem from that of Namba. The procedure adopted here is a direct extension of the kernel-function methods developed for use in isolated airfoil theory. It also allows analytical expressions to be derived for the required spanwise and chordwise integrations, thus affording greater accuracy and improved efficiency over schemes that employ numerical quadrature exclusively.

The next section presents the governing integral equation, along with the basic flow model and assumptions on which it is based. Section III describes the solution procedure, and numerical results and comparisons with other theories are presented and discussed in Sec. IV.

II. Flow Model and Governing Integral Equation

In the model, the blade row is assumed to be housed in an infinitely long, hard-walled annular duct of constant hub/tip ratio h, containing a uniform subsonic axial flow at Mach number M, as shown in Fig. 1. The flow is assumed to be inviscid and steady in blade-fixed coordinates. In this reference frame, the inflow has a relative velocity $U_R = [U^2 + (\omega r)^2]^{1/2}$, and follows the helical undisturbed stream surfaces defined by $\zeta = \theta - (\omega/U)z = \text{const}$. The blades are assumed to produce only small perturbations about this undisturbed flow, allowing the linearized boundary conditions to be applied along these surfaces. The inviscid and small perturbation assumptions further imply that the disturbance flowfield is irrotational, and hence isentropic. We restrict ourselves here to considering only the case where the undisturbed relative Mach number at the tip is subsonic. This ensures that all disturbances will damp out far upstream of the rotor, and that far downstream only the trailing vortices will remain.

Since the problem has been linearized, the disturbance fields produced by blade thickness and loading may be determined separately and then superimposed. However, this separation is not as straightforward as it is for a planar, isolated airfoil. In the thickness part of the rotor problem, the blades must be cambered to achieve the condition of zero loading. This zero-loading camber line, or "thickness-induced camber," can be calculated as an integral over the known source distribution once the blade thickness and the operating conditions are prescribed. A more thorough discussion of this point, as well as sample calculations, can be found in Refs. 13 and 14. In the idealized case of infinitely thin blades, the present loading analysis can be applied directly without consideration of this effect. However, for blades of finite thickness, the analysis assumes that the thickness-induced camber has been calculated and combined with the geometric camber to give the net camber line distribution used in the subsequent boundary condition.

The derivation of the governing integral equation for the lifting-surface analysis is somewhat lengthy, and since it appears elsewhere,[13,15] will not be repeated here except for a brief outline to introduce some concepts. The first step is the manipulation of the linearized flow equations into a single equation for the perturbation pressure p. This is essentially a Prandtl-Glauert equation, written in the rotating, three-dimensional, cylindrical coordinate system depicted in Fig. 1. A singular solution to this equation, or Green's function, is found which physically represents an idealized point

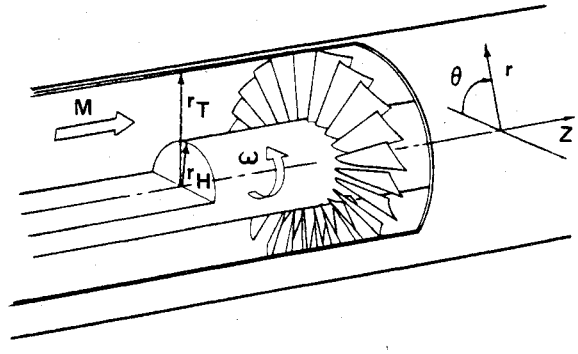

Fig. 1 Blade row and duct geometry.

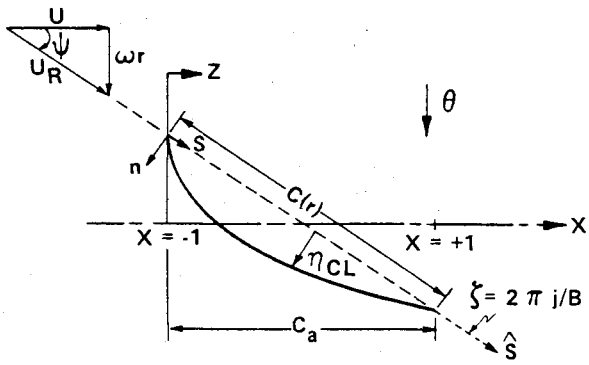

Fig. 2 Camber line geometry in blade-fixed coordinates.

force/volume acting on the fluid. This will be referred to as the pressure dipole solution.

To obtain the pressure field for the entire blade row, these singularities are distributed along the undisturbed stream surfaces $\zeta_j = (2\pi j)/B$, $j = 0,1 \ldots B-1$, (see Fig. 2) with the dipole's strength equal to the local loading, $\Delta p(r_0,s_0)$. On a blade surface s_0 is uniquely related to z_0, and so we set $\Delta p(r_0,s_0(z_0)) = \Delta p(r_0,z_0)$ and transform the chordwise integration to one over the axial coordinate. The resulting expression is

$$p(r,\zeta,z) = \frac{\omega B}{\pi\beta^2 U(1-h^2)r_T^2}$$

$$\times \int_0^{c_a}\int_{r_H}^{r_T} r_0 \Delta p(r_0,z_0) H(z-z_0)\,dz_0 dr_0$$

$$+ \frac{B}{4\pi\beta^2 r_T^2}\int_0^{c_a}\int_{r_H}^{r_T}\sum_{m=-\infty}^{\infty}\sum_{k=1}^{\infty}\frac{R_{mBk}(\sigma)R_{mBk}(\sigma_0)e^{imB\zeta}}{\omega\lambda_{mBk}/U}$$

$$\times \exp[\Lambda_{mBk}(z,z_0)(z-z_0)]V_{mBk}(r_0,z,z_0)\Delta p(r_0,z_0)\,dz_0 dr_0 \tag{1}$$

where

$$\lambda_{mBk} = \frac{|mB|U}{\omega r_T \beta^2}\sqrt{\beta^2\left(\frac{K_{mBk}}{mB}\right)^2 - \left(\frac{\omega r_T}{a_{-\infty}}\right)^2} \tag{2a}$$

$$\Lambda_{mBk}(z,z_0) = \frac{\omega}{U}\left[\frac{imB}{\beta^2} - \lambda_{mBk}\,\mathrm{sgn}(z-z_0)\right] \tag{2b}$$

$$V_{mBk}(r_0,z,z_0) = \frac{imB}{r_0} - \frac{\omega^2 r_0}{U^2}\left[imB\frac{M^2}{\beta^2} - \lambda_{mBk}\,\mathrm{sgn}(z-z_0)\right] \tag{2c}$$

and the remaining symbols are defined in the Nomenclature. It has been assumed for convenience in Eq. (1) that the axial projection of the blade chord c_a is independent of radius, though this is not essential to the analysis. Equation (1) has been shown to yield a pressure field that is continuous everywhere except across the blades,[15] and satisfies the same hard-wall boundary condition imposed on the pressure dipole solution,

$$\partial p/\partial r = 0 \text{ at } r = r_H, r_T \tag{3}$$

Inspection of the linearized radial momentum equation shows that Eq. (3) is equivalent to requiring that the radial velocity vanish at the hub and tip.

The preceding result is a superposition of duct modes that are sinusoidal in θ with a fundamental period $2\pi/B$, have a complex exponential dependence on z, and whose radial variation is described by the radial eigenfunctions R_{mBk} and their associated eigenvalues K_{mBk}. The R_{mBk} denote linear combinations of Bessel functions of the first and second kind that satisfy Eq. (3). Their argument is actually $K_{mBk}\sigma$, which is written here simply as σ for the sake of brevity. These functions are described at length by McCune.[1-3]

Knowing p, the normal component of the disturbance velocity v_n (see Fig. 2) can be obtained by integrating the corresponding momentum equation from upstream infinity along the undisturbed helical streamline through (r,ζ,z). This result is[13,15]

$$v_n(r,\zeta,z) = \frac{B\left(\frac{\omega r}{U}\right)^2}{\pi\rho_{-\infty}U_R r\beta^2(1-h^2)r_T^2}$$

$$\times \int_0^{c_a}\int_{r_H}^{r_T} r_0 \Delta p(r_0,z_0) H(z-z_0)\,dz_0 dr_0$$

$$- \frac{B\left[1+\left(\frac{\omega r}{U}\right)^2\right]^{1/2}}{2\pi\rho_{-\infty}U_r}\left\{\int_0^{c_a}\Delta p(r,z_0)H(z-z_0)\,dz_0\right.$$

$$- \sum_{\substack{m=-\infty\\ \neq 0}}^{\infty}\sum_{k=1}^{\infty}\frac{R_{mBk}(\sigma)e^{imB\zeta}}{(mB)^2\left[\left(\frac{K_{mBk}}{mB}\right)^2+\left(\frac{\omega r_T}{U}\right)^2\right]}$$

$$\left.\times \int_0^{c_a}\int_{r_H}^{r_T}\left(r_0\frac{\partial^2\Delta p}{\partial r_0^2} + \frac{\partial \Delta p}{\partial r_0}\right)R_{mBk}(\sigma_0)H(z-z_0)\,dz_0 dr_0\right\}$$

$$+ \frac{B}{4\pi\beta^2 r_T^2\rho_{-\infty}U_R}\int_0^{c_a}\int_{r_H}^{r_T}\sum_{m=-\infty}^{\infty}\sum_{k=1}^{\infty}$$

$$\times \frac{R_{mBk}(\sigma)R_{mBk}(\sigma_0)e^{imB\zeta}}{\omega\lambda_{mBk}/U}V_{mBk}(r_0,z,z_0)$$

$$\times\left\{\frac{\omega r}{U} - \frac{imB}{r\Lambda_{mBk}(z,z_0)}\left[1+\left(\frac{\omega r}{U}\right)^2\right]\right\}$$

$$\times \exp[\Lambda_{mBk}(z,z_0)(z-z_0)]\Delta p(r_0,z_0)\,dz_0 dr_0 \tag{4}$$

Note that the terms in the first five lines of Eq. (4) are identically zero upstream of the blade row. The first three lines represent contributions from the $m = 0$, $k = 0$ mode. The next term, which involves radial derivatives of the loading, represents the influence of the trailing vortex pattern. For fixed ζ, this term is independent of z downstream of the blade row, which reflects the fact that the vortices are convected downstream without attenuation along the undisturbed streamlines. This will be referred to subsequently as the wake term.

In the last group of terms, since we have assumed $M_R < 1$ everywhere, one can easily show that λ_{mBk} from Eq. (2a) is always real and positive. Hence, these terms rapidly attenuate as one moves away from the blade row, and will be referred to subsequently as the exponentially decaying terms. When the tip relative Mach number becomes supersonic, certain modes will propagate undamped down the duct. This was first noted by McCune,[1-3] who was thus able to relate the resulting acoustic radiation directly to the blade thickness distribution. Such modes are identical in form to the propagating duct acoustic modes studied by Tyler and Sofrin,[16] which have since formed the basis for numerous investigations of turbomachinery noise.

To convert Eq. (4) into the desired integral equation, the right-hand side is specialized to the reference blade surface, $\zeta = 0$. It is also convenient for machine calculations to rationalize the resulting expression so that only real arithmetic

is involved. From here on, we will work with the following dimensionless coordinates

$$\sigma = r/r_T \qquad h \le \sigma \le 1 \tag{5a}$$

$$x = \frac{z - c_a/2}{c_a/2} \qquad -1 \le x \le 1 \tag{5b}$$

and parameters

$$\phi_T = \omega r_T / U \qquad \eta_T = c_a / 2 r_T \tag{6a}$$

One can express the aspect ratio and a solidity parameter based on the constant axial chord projection c_a in terms of these dimensionless groups

$$\text{aspect ratio} = (r_T - r_H)/c_a = (1-h)/2\eta_T \tag{6b}$$

$$\text{solidity at tip} = Bc_a/2\pi r_T = B\eta_T/\pi \tag{6c}$$

As a convenient shorthand, we also define

$$A_{mBk} = \left(\frac{K_{mBk}}{mB}\right)^2 + \phi_T^2 \qquad m \neq 0 \tag{7a}$$

$$B_{mBk} = \left[\left(\frac{K_{mBk}}{mB}\right)^2 - \left(\frac{\phi_T M}{\beta}\right)^2\right]^{1/2} \qquad m \neq 0 \tag{7b}$$

in terms of which λ_{mBk} becomes

$$\lambda_{mBk} = \frac{mB}{\beta\phi_T} B_{mBk} \qquad m \neq 0$$

$$= \frac{K_{0k}}{\beta\phi_T} \qquad m = 0 \tag{7c}$$

The loading is nondimensionalized by the dynamic pressure associated with the uniform axial velocity,

$$\Delta\hat{p} = \Delta p / \tfrac{1}{2}\rho_{-\infty} U^2 \tag{8}$$

The left-hand side of Eq. (4) is related to the blade geometry as follows. Let $\mathfrak{R}_{CL}(s,r)$ denote the function describing the blade camber line as a function of streamline and radial coordinates (see Fig. 2), after accounting for any thickness-induced camber as noted previously. Then the blade boundary condition requires that

$$v_n(\zeta = 0) = U_R \frac{\partial \mathfrak{R}_{CL}}{\partial s}\bigg)_r = U_R \frac{\partial \hat{\mathfrak{R}}_{CL}}{\partial \hat{s}}\bigg)_\sigma \tag{9}$$

where we have nondimensionalized $\mathfrak{R}_{CL}$ and s by the local semichord

$$\hat{\mathfrak{R}}_{CL} = \frac{\mathfrak{R}_{CL}}{c/2} \qquad \hat{s} = \frac{s - c/2}{c/2} \tag{10}$$

On the reference blade $z = s\cos\psi$, where $\psi = \tan^{-1}(\phi_T\sigma)$ is the local undisturbed flow angle (Fig. 2), and $c_a = c\cos\psi$. It then follows from the definitions in Eqs. (5) and (10) that $\hat{s} = x$.

With the preceding definitions, the integral equation relating the blade camber line to the unknown loading can be written as

$$\frac{\partial \hat{\mathfrak{R}}_{CL}}{\partial \hat{s}}\bigg)_\sigma = \frac{B\eta_T\phi_T^2\sigma}{2\pi\beta^2(1-h^2)(1+\phi_T^2\sigma^2)} \int_{-1}^{x} dx_0 \int_h^1 d\sigma_0 \Delta\hat{p}(\sigma_0, x_0)\sigma_0 - \frac{B\eta_T}{4\pi\sigma}\left\{\int_{-1}^{x} \Delta\hat{p}(\sigma, x_0)\,dx_0 - 2\sum_{m=1}^{\infty}\sum_{k=1}^{\infty} \frac{R_{mBk}(\sigma)}{(mB)^2 A_{mBk}}\right.$$

$$\left. \times \int_{-1}^{x} dx_0 \int_h^1 d\sigma_0 \left(\sigma_0 \frac{\partial^2 \Delta\hat{p}}{\partial\sigma_0^2} + \frac{\partial \Delta\hat{p}}{\partial\sigma_0}\right) R_{mBk}(\sigma_0)\right\} + \frac{B\eta_T\phi_T^2\sigma}{8\pi\beta^2(1+\phi_T^2\sigma^2)} \int_{-1}^{+1} dx_0 \int_h^1 d\sigma_0 \sum_{k=1}^{\infty} R_{0k}(\sigma) R_{0k}(\sigma_0)\sigma_0 \Delta\hat{p}(\sigma_0, x_0)\,\mathrm{sgn}(x - x_0)$$

$$\times \exp\left[-\frac{K_{0k}\eta_T}{\beta}|x - x_0|\right] + \frac{B\eta_T\phi_T^2}{4\pi\beta^2(1+\phi_T^2\sigma^2)} \int_{-1}^{+1} dx_0 \int_h^1 d\sigma_0 \sum_{m=1}^{\infty}\sum_{k=1}^{\infty} R_{mBk}(\sigma) R_{mBk}(\sigma_0)\Delta\hat{p}(\sigma_0, x_0)$$

$$\times \exp\left[-\frac{mB\eta_T}{\beta} B_{mBk}|x - x_0|\right]\left\{[C^+\sigma_0 + C^-\sigma_0^{-1}]\mathrm{sgn}(x - x_0)\cos\frac{mB\phi_T\eta_T}{\beta^2}(x - x_0) + [S^+\sigma_0 + S^-\sigma_0^{-1}]\sin\frac{mB\phi_T\eta_T}{\beta^2}(x - x_0)\right\} \tag{11a}$$

To facilitate the solution procedure described in Sec. III, like powers of σ_0 have been grouped together in the exponentially decaying terms. The coefficients of $\sigma_0^{\pm 1}$ in these terms are given by

$$C^+ = \sigma - \frac{\beta^2(1+\phi_T^2\sigma^2)}{\sigma A_{mBk}} \qquad C^- = -\frac{\beta^2(1+\phi_T^2\sigma^2)}{\phi_T^2\sigma A_{mBk}}$$

$$S^+ = -\phi_T\beta\left[\frac{M^2\beta_R^2}{\sigma\beta^4} + \sigma\left(1 + \frac{\beta_R^2}{\beta^2\phi_T^2\sigma^2}\right)B_{mBk}^2\right]\Big/ A_{mBk}B_{mBk}, \quad S^- = +\phi_T\beta\left[\frac{\beta_R^2}{\sigma\beta^2\phi_T^2} - \frac{\sigma}{\phi_T^2}B_{mBk}^2\right]\Big/ A_{mBk}B_{mBk} \tag{11b}$$

As noted in the Introduction, this integral equation does not agree with that derived by Namba. The differences can be traced back to the solution for the pressure field, Eq. (1). Namba's expression for p [Ref. 10, Eq. (15)] quotes a different form for the $m = 0$, $k = 0$ term, and also contains a "scale factor," $\Lambda(\rho)$ in his terminology, which does not appear in our result.

For a discussion of the singularities which can arise in the integrand of Eq. (11), the reader is referred to Refs. 17 and 18.

III. Solution Procedure

In order to solve the integral equation, it is assumed that the unknown loading can be expanded in a finite series of suitably chosen chordwise and spanwise loading functions. Specifically, we set

$$\Delta\hat{p}(\sigma_0,x_0) = \sum_{i=1}^{NI}\sum_{j=1}^{NJ} a_{ij}\sigma_0^{j-1}f_i(x_0) \tag{12a}$$

where

$$f_i(x_0) = \sqrt{\frac{1-x_0}{1+x_0}} \qquad i=1, \qquad f_i(x_0) = \sin[(i-1)\cos^{-1}x_0] \qquad i\geq 2 \tag{12b}$$

and the a_{ij}, $i=1,2...NI$, $j=1,2...NJ$, are constants to be determined by the solution. The chordwise functions are the same as those often used in subsonic airfoil theory. They automatically satisfy the Kutta condition at the trailing edge, $x_0=+1$, and the $i=1$ term exhibits the appropriate square root singularity at the leading edge, $x_0=-1$. The polynomial variation in σ_0 allows simple treatment of the boundary condition in Eq. (3), as well as the radial derivatives in the wake term.

Substitution of Eq. (12) into Eq. (11a) leads to radial integrations of the form

$$\int_h^1 \sigma_0^j \mathrm{d}\sigma_0 = \frac{1-h^{j+1}}{j+1} \equiv I^j \qquad j=0,1... \tag{13a}$$

$$\int_h^1 \sigma_0^j R_{mBk}(K_{mBk}\sigma_0)\,\mathrm{d}\sigma_0 \equiv I^j_{mBk} \qquad \begin{matrix} j=-1,\,0,\,1... \\ m=0...\infty \\ k=1...\infty \end{matrix} \tag{13b}$$

The axial integrations which result are:

$$\int_{-1}^{x} f_i(x_0)\,\mathrm{d}x_0 \equiv C^i(x) \tag{14a}$$

$$\int_{-1}^{+1} f_i(x_0)\,\mathrm{sgn}(x-x_0)\exp[-K_{0k}\eta_T|x-x_0|/\beta]\mathrm{d}x_0 \equiv C^i_{0k}(x) \tag{14b}$$

$$\int_{-1}^{+1} f_i(x_0)\,\mathrm{sgn}(x-x_0)\cos\left[\frac{mB\phi_T\eta_T}{\beta^2}(x-x_0)\right]\exp[-mB\eta_T B_{mBk}|x-x_0|/\beta]\mathrm{d}x_0 \equiv C^i_{mBk}(x) \tag{14c}$$

$$\int_{-1}^{+1} f_i(x_0)\sin\left[\frac{mB\phi_T\eta_T}{\beta^2}(x-x_0)\right]\exp[-mB\eta_T B_{mBk}|x-x_0|/\beta]\mathrm{d}x_0 \equiv S^i_{mBk}(x) \tag{14d}$$

It so happens that both the radial and axial integrations defined in Eqs. (13) and (14) can be performed analytically, which is a great advantage over schemes requiring numerical quadrature. The resulting formulas and their derivations are too lengthy to give here; the interested reader can find an outline of the steps involved and the final results in Ref. 17 or 18.† For the present it is assumed that these integrals are all known.

Next we choose a set of collocation points (σ_n,x_ℓ), $n=1,2...NN$, $\ell=1,2...NL$, at which to evaluate Eq. (11), and define

$$b_{n\ell} = \frac{\partial\hat{\mathfrak{V}}_{CL}}{\partial\hat{s}}(\sigma_n,x_\ell) \tag{15}$$

Substituting Eqs. (12-15) into Eq. (11) reduces the integral equation to the following set of simultaneous linear algebraic equations for the a_{ij}'s

$$\sum_{i=1}^{NI}\sum_{j=1}^{NJ} U_{ij}(\sigma_n,x_\ell)a_{ij} = b_{n\ell} \qquad n=1,2...NN \qquad \ell=1,2...NL \tag{16}$$

where $NN\times NL = NI\times NJ$ for the system to be determinant. The elements of the matrix U represent the dimensionless upwash produced at point (σ_n,x_ℓ) by the (i,j) loading function. These are given by

$$\begin{aligned} U_{ij}(\sigma_n,x_\ell) = {} & \frac{B\eta_T\phi_T^2\sigma_n}{2\pi\beta^2(1-h^2)(1+\phi_T^2\sigma_n^2)}C^i(x_\ell)I^j - \frac{B\eta_T}{4\pi\sigma_n}\left[C^i(x_\ell)\sigma_n^{j-1} - 2(j-1)^2C^i(x_\ell)\sum_{m=1}^{NM}\sum_{k=1}^{NK}\frac{R_{mBk}(\sigma_n)I^{j-2}_{mBk}}{(mB)^2A_{mBk}}\right] \\ & + \frac{B\eta_T\phi_T^2\sigma_n}{8\pi\beta^2(1+\phi_T^2\sigma_n^2)}\sum_{k=1}^{NK}C^i_{0k}(x_\ell)R_{0k}(\sigma_n)I^j_{0k} + \frac{B\eta_T\phi_T^2}{4\pi\beta^2(1+\phi_T^2\sigma_n^2)}\sum_{m=1}^{NM}\sum_{k=1}^{NK}R_{mBk}(\sigma_n) \\ & \times[(C^+(\sigma_n)I^j_{mBk} + C^-(\sigma_n)I^{j-2}_{mBk})C^i_{mBk}(x_\ell) + (S^+(\sigma_n)I^j_{mBk} + S^-(\sigma_n)I^{j-2}_{mBk})S^i_{mBk}(x_\ell)] \end{aligned} \tag{17}$$

where NM and NK are the terms at which the m and k series are truncated, respectively.

†The axial integrals are found to be expressible as an infinite series involving modified Bessel functions. At high solidity or large values of m and k, accuracy in the summation is lost through computer roundoff error; the reason this occurs is discussed in Refs. 17 and 18. In such cases, numerical quadrature was used.

Before solving the matrix equation in Eq. (16), one more feature of the solution needs to be considered; namely, the hard-wall boundary condition in Eq. (3) requires that $\Delta\hat{p}$ have zero spanwise derivative at the hub and tip. This condition can be enforced automatically as follows. If Eq. (12) is differentiated with respect to σ_0, and the resulting expression set equal to zero at $\sigma_0 = h$ and 1, two equations involving the a_{ij} will follow. Simultaneous satisfaction of these two equations will, in general, depend on x_0. But if it is required that they be satisfied for all $|x_0| \le 1$, and for each i individually, then $a_{i,NJ-1}$ and $a_{i,NJ}$ can be solved for uniquely

$$a_{i,NJ-1} = \sum_{j=2}^{NJ-2} d_j a_{ij} \quad d_j = -\frac{(j-1)(1-h^{j-NJ})}{(NJ-2)(1-h^{-1})} \tag{18a}$$

$$a_{i,NJ} = \sum_{j=2}^{NJ-2} e_j a_{ij} \quad e_j = -\frac{(j-1)(1-h^{j-NJ+1})}{(NJ-1)(1-h)} \tag{18b}$$

In effect, for each value of i Eq. (3) has been used to express two of the radial coefficients in terms of the remaining $(NJ-2)$.

Upon substituting Eq. (18) into Eq. (16), one obtains an altered matrix equation of the form

$$\sum_{i=1}^{NI} \sum_{j=1}^{NJ-2} U'_{ij}(\sigma_n, x_\ell) a_{ij} = b_{n\ell} \quad n = 1,2...NN \quad \ell = 1,2...NL \tag{19a}$$

where the elements of the modified matrix U' are given by

$$\begin{aligned} U'_{ij}(\sigma_n, x_\ell) &= U_{ij}(\sigma_n, x_\ell) \quad j = 1 \\ &= U_{ij}(\sigma_n, x_\ell) + d_j U_{i,NJ-1}(\sigma_n, x_\ell) \\ &\quad + e_j U_{i,NJ}(\sigma_n, x_\ell) \quad 2 \le j \le NJ-2 \end{aligned} \tag{19b}$$

Note that the $j = 1$ terms remain unaffected, since they satisfy the required condition trivially. Since the number of unknowns in Eq. (19a) has effectively been reduced to $NI \times (NJ-2)$, the number of collocation points should be reduced accordingly. In view of how Eq. (18) was derived, the most logical approach would be to reduce the number of spanwise stations in order to get $NN \times NL = NI \times (NJ-2)$. Once having set up the matrix equation, its solution was carried out by using Gaussian elimination with pivoting. This yields a_{ij} for all i and $j = 1...NJ-2$; the $a_{i,NJ-1}$ and $a_{i,NJ}$ are then obtained from Eq. (18).

The local loading $\Delta\hat{p}$ at any point on the blades is calculated from Eq. (12). The form of that equation also allows simple algebraic expressions to be derived for the sectional lift and moment coefficients, the overall torque and axial force coefficients, the static and total pressure rise, and the turning produced by the rotor. These results are omitted here for brevity, but can be found in Refs. 17 and 18.

IV. Numerical Results and Discussion

A computer program implementing the solution procedure just described has been developed using double precision arithmetic throughout so as to minimize the influence of round-off error. Seven cases have been run thus far to test the program over a broad range of operating conditions, as specified by the input parameters B, h, M, ϕ_T and η_T. Table 1 summarizes the values used for each case, along with a brief description of the specified camber line.

The first three cases were designed to test the present theory against a two-dimensional strip theory at a high hub/tip ratio, where one would expect strip theory to provide a reasonable approximation. Similar comparisons are drawn in cases 4 and 5 for a low hub/tip ratio, for which three-dimensional effects are much more significant. Finally, cases 6 and 7 provide comparisons with the inverse three-dimensional theory of Okurounmu and McCune.[5,6]

In each case, $NI = 5$ chordwise and $NJ = 5$ spanwise loading functions were used to represent $\Delta\hat{p}$. Along the chord, $NL = 5$ collocation stations were used in all cases. For cases 1-5 these were evenly distributed between the leading and trailing edges, i.e., at $x = \pm 0.66$, ± 0.33, and 0.0. In cases 6 and 7 it was found necessary to redistribute the points nearer to the edges of the blades, as will be discussed later. In the spanwise direction, each case used $NN = 3$ collocation stations, equally spaced between the hub and tip, with the hard-wall boundary condition enforced at the hub and tip as described in Sec. III. The number of azimuthal modes included in the calculation, NM, was 10 in all cases; the number of radial modes included, NK, was set at 20 or 30 depending on whether h was 0.8 or 0.5, respectively.

The computer running times required for cases 1-7 varied between 10 and 20 min on an IBM 360/65, using the G compiler. By far the majority of that time is spent in evaluating the axial integrals. The time needed for their evaluation is primarily dictated by the number of integrals which can be done analytically before round-off error becomes a problem.[17,18] As a result, the running time can be expected to increase along with the solidity. However, the coefficient matrix in Eq. (19) depends only on the first five parameters in Table 1. The program has provision for storing the matrix on tape, so that subsequent calculations for the same operating conditions, but different blade camber lines, e.g., cases 1 and 2, 4 and 5, 6 and 7, can be performed in a matter of seconds.

A. Comparisons with Two-Dimensional Strip Theory

In case 1, the camber line was specified to be a flat plate at each radial station; however, a radial twist is imparted to the blades such as to hold the local angle of attack, α_{3D}, constant at + 5 deg. The high hub/tip ratio in this case suggests that the loading might be predicted reasonably well by application of a two-dimensional strip theory. For the latter, use was made of the closed-form analytical results of Pistolesi[19] for a flat plate cascade in incompressible flow, after first correcting for compressibility effects via the appropriate Prandtl-Glauert transformation[20]; details on exactly how these were applied can be found in Refs. 17 and 18.

Table 1 Input parameters for cases 1-7

Case	B	$h = r_H/r_T$	Axial Mach no.	$\phi_T = \omega r_T/U$	$\eta_T = c_a/2r_T$	Camber line shape
1	50	0.8	0.5	1.0	0.03	Flat plate; $\alpha_{3D} = 5$ deg, const
2	50	0.8	0.5	1.0	0.03	10% parabolic-arc camber; $\alpha_{3D} = 0$ deg
3	50	0.8	0.5	1.0	0.06	Flat plate; $\alpha_{3D} = 5$ deg, const
4	30	0.5	0.5	1.0	0.05	Flat plate; $\alpha_{3D} = 5$ deg, const
5	30	0.5	0.5	1.0	0.05	Flat plate; $\alpha_{3D}(h) = 10$ deg, $\alpha_{3D}(1) = 0$ deg
6	40	0.8	0.5	1.497	0.0833	Free vortex design
7	40	0.8	0.5	1.497	0.0833	Design for 20% variation in Γ

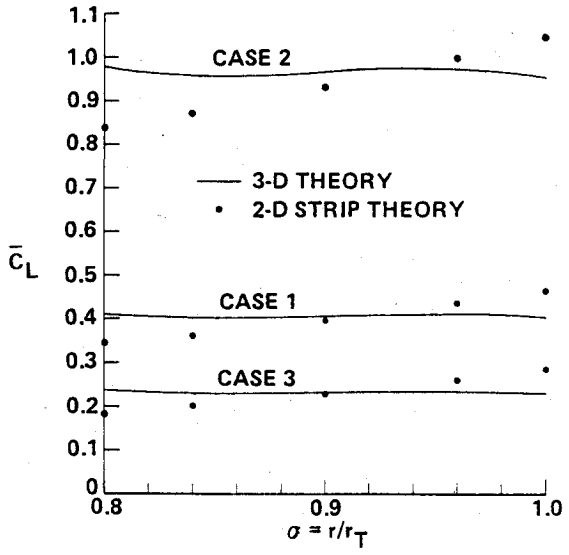

Fig. 3 Comparison of present three-dimensional theory and two-dimensional strip theory for high hub/tip ratio.

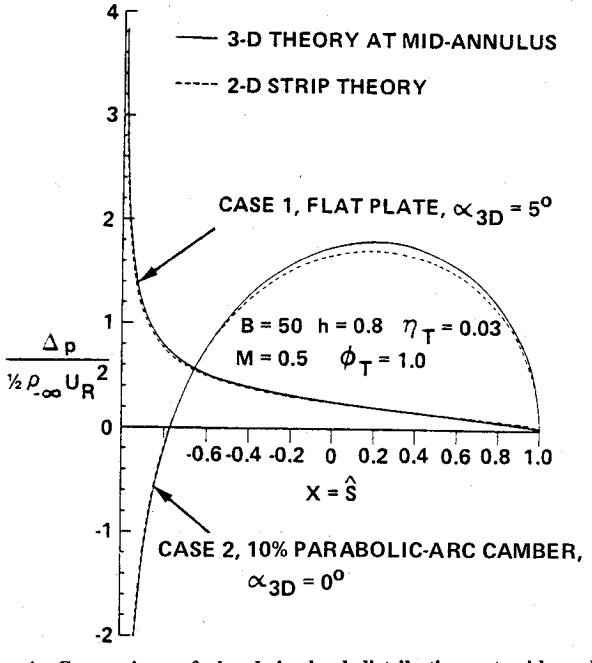

Fig. 4 Comparison of chordwise load distributions at midannulus for high hub/tip ratio.

At each spanwise station, the strip theory predicts the sectional lift coefficient defined by

$$\bar{C}_L = L(\sigma) / \tfrac{1}{2}\rho_{-\infty} U_R^2 c \qquad (20)$$

This is compared in Fig. 3 with the predictions of the present three-dimensional theory. When viewing these and subsequent results for $\bar{C}_L$ it should be kept in mind that the spanwise variation in L will be even greater, since the local dynamic pressure and chord both increase with radius. The agreement between the two calculations is seen to be quite good at midannulus. However, whereas the strip theory predicts a 35% increase in $\bar{C}_L$ from hub to tip, the three-dimensional results show little variation. The corresponding changes in the circulation Γ from hub to tip are +67 and 19%, respectively. Thus, significant trailing vortex effects can be expected despite the high hub/tip ratio; their influence will be discussed at more length shortly. The low solidity in this case, roughly

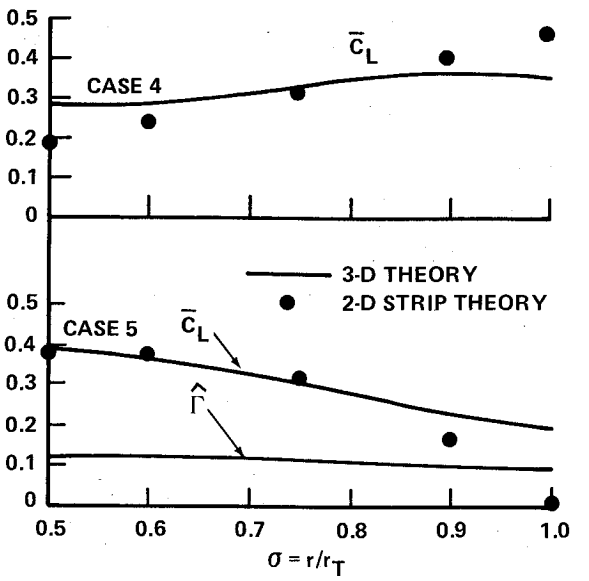

Fig. 5 Comparison of present three-dimensional theory and two-dimensional strip theory for low hub/tip ratio.

two-thirds at midannulus, suggests that the chordwise load distribution should closely approximate that of an isolated flat plate. This comparison is shown in Fig. 4, and the agreement is seen to be excellent.

In case 2, the blades are assumed to have zero angle of attack relative to the inflow velocity and a parabolic-arc camber line; otherwise, the input parameters are the same as in case 1. The ratio of maximum camber to the local chord length is taken to be 0.10, and constant with radius. As in case 1, one would expect that the high hub/tip ratio and low solidity would cause the three-dimensional results to approach those for a two-dimensional isolated airfoil. Such a comparison for case 2 is also shown in Fig. 3. Again, good agreement is shown at midannulus, while the strip theory significantly overestimates the lift near the tip, and underestimates it near the hub. The comparison of chordwise load distribution at midannulus is shown in Fig. 4, and again very good agreement is obtained.

For case 3, η_T, and hence the solidity all across the annulus, has been doubled; the other input parameters and the camber line are the same as in case 1. This case thus provides a better check on whether the present program correctly predicts blade interference effects. Its predictions and those from the strip theory are also compared in Fig. 3. The higher solidity is seen to result in an overall reduction in loading. Again very good agreement between the two theories is exhibited at midannulus, with discrepancies at other stations following the same trends seen in cases 1 and 2.

The three cases just discussed were chosen to assess the agreement between the present analysis and strip theory for high hub/tip ratio. The conditions for case 4 were chosen to exhibit more significant three-dimensional effects, with the hub/tip ratio reduced to 0.5 and B reduced to 30; the other parameters and the camber line are the same as in case 1. The results and the comparison with strip theory are shown in Fig. 5. Both calculations show larger radial variations than in the previous cases, as expected. Again, the strip theory significantly underestimates the loading at inboard stations, and overestimates it near the tip, with good agreement at midannulus. However, the percentage errors relative to the three-dimensional predictions are much greater in this case than in the previous cases with high hub/tip ratio.

In all four cases discussed thus far, it is seen that the present three-dimensional theory and a two-dimensional strip theory show good agreement only near midannulus. The strip theory tends to underestimate the loading near the hub and

overestimate it near the tip, even when the hub/tip ratio is fairly high. McCune and Dharwadkar[7] have found the same trend in their study of the three-dimensional lifting-line approximation. Such behavior can be explained on the following basis. The circulation in the preceding cases is monotonically increasing from hub to tip; hence the trailing vorticity behind the blades is of the same sign all along the span. The angle of attack induced at the blades by this vorticity [i.e., the wake terms in Eqs. (11a) and (17)] is positive near the hub and negative near the tip. Since strip theory neglects this effect, the discrepancies noted previously result; at midannulus, the effects of the vortices on either side are largely self-cancelling, and strip theory does rather well.

If the preceding argument is valid, then if Γ were to decrease with radius, the discrepancy between the two theories should reverse. This was the purpose in running the somewhat contrived case 5, which is the same as case 4, except that α_{3D} was specified to decrease linearly from 10 deg at the hub to 0 deg at the tip. The results are compared with strip theory in Fig. 5; to augment the discussion, the dimensionless circulation, $\hat{\Gamma}=\Gamma/(UL_{\theta T})$, is also displayed. The latter is seen to be very nearly constant over the inner half of the span, and drops by about 25% over the outer half. The lift coefficient is well predicted by strip theory in that region where $d\Gamma/dr$ is small (weak trailing vorticity). But over the outer span where $d\Gamma/dr$ is negative, strip theory now significantly underestimates the loading, in accordance with the preceding argument. Hence it appears that the three-dimensional effects of trailing vorticity act in such a way as to reduce spanwise variations relative to those predicted by strip theory.

B. Comparison with Inverse Three-Dimensional Theory

The remaining two cases, 6 and 7, are of particular interest because they provide comparisons between the present work and another three-dimensional lifting-surface theory, that of Okurounmu and McCune.[5,6] In contrast to the off-design problem considered here, they solved the design problem, i.e., the determination of that camber line that will produce a specified load distribution. They presented plots of camber line slope vs chordwise distance which were input to our program to see if the predicted load agreed with the loading distribution specified in the design calculation. The camber line slopes had been normalized by the overall static pressure rise coefficient, c_{ps}, as defined in Eq. (24) of Ref. 18. This quantity was assumed to be unity in reading their curves; ideally then, the present program should predict this value of c_{ps} as part of the results.

Two calculations were performed; the first was for a free-vortex design (case 6), in which by definition the circulation about the blades, Γ, was constant with radius. (Okurounmu and McCune refer to this as the constant-work case.) In the second (case 7), the circulation varied by 20% from hub to tip, referenced to its radius-weighted mean over the span. Except for the camber line geometry, all other parameters input to the program were identical in cases 6 and 7 (Table 1); hence, each required the inversion of the same upwash coefficient matrix. In both cases, the design total pressure ratio was between 1.10 and 1.15.

Cases 6 and 7 were originally run with the same axial collocation stations used in cases 1-5 (see Refs. 17 and 18, where these results appear as cases 5 and 6, respectively). The predicted and design load distributions were in good agreement for the free-vortex case, but not for case 7, in which Γ varied with radius. For the latter, the present theory significantly overestimated the load all along the span. It was later realized that the high solidity of the blade row, $c/L_\theta \simeq 2$, is forcing the problem toward the limit of a channel flow. That is, the fluid is constrained to exit the blade row at an angle very nearly equal to the camber line slope at the trailing edge. Thus the net turning, from which the loading can be inferred, is determined almost solely by the slopes at the trailing edge; yet the rearward most collocation station was a sixth of a chord upstream of this plane.

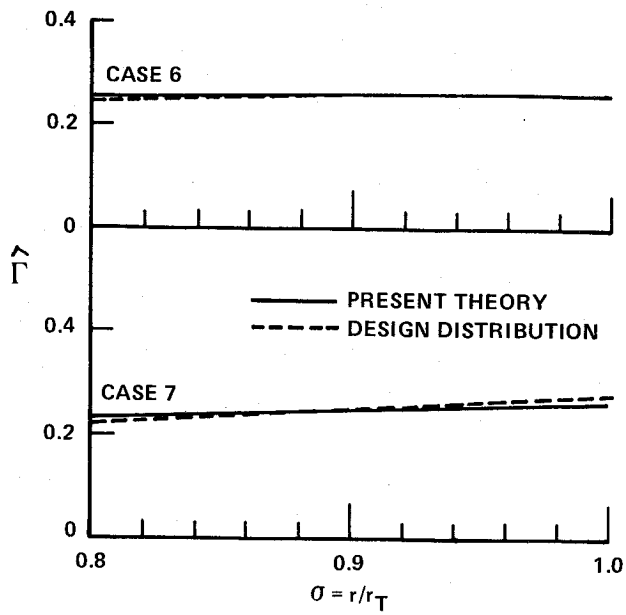

Fig. 6 Comparison of present theory with Okurounmu and McCune's design distribution of spanwise loading.

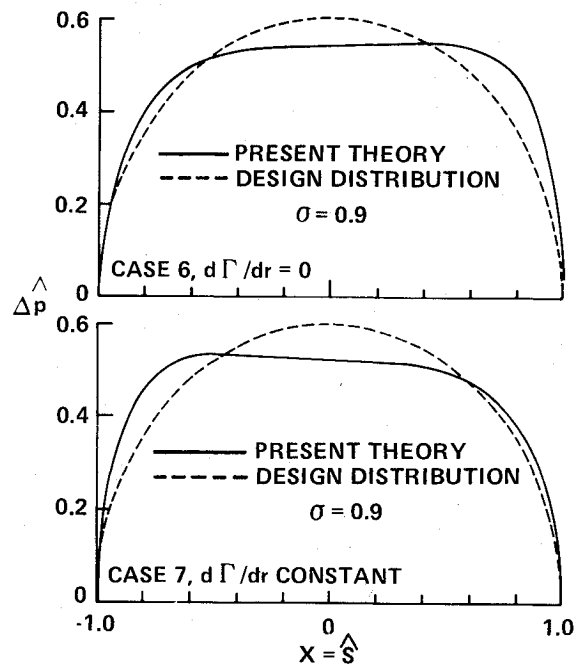

Fig. 7 Comparison of present theory with Okurounmu and McCune's design distribution of chordwise loading.

Accordingly, case 7 was rerun with the same number of collocation points, but with their axial positions moved closer to the edges, at $x=\pm 0.8$, ± 0.4 and 0.0. This increased the agreement dramatically; c_{ps} dropped from a value of 1.54 with the old points to 0.98 with the new. Case 6, the free-vortex design for which the original points gave good agreement,[17,18] was also rerun; with the new points, the agreement was enhanced somewhat, with c_{ps} dropping from 1.04 to 1.01. Apparently, the reason that shifting the points has a much more dramatic effect in case 7 than in case 6 is because the camber line slopes near the trailing edge are changing more rapidly in the former case than in the latter.[5,6]

The static pressure rise coefficient c_{ps} only reflects the integrated effect of the loading. The radial variation of the predicted dimensionless circulation $\hat{\Gamma}$ is compared with the distributions prescribed by Okurounmu and McCune[5,6] for

both cases in Fig. 6. Good agreement is exhibited over the entire span. An even more sensitive comparison can be made between the predicted and prescribed chordwise load distributions; the latter was proportional to $(1-x^2)^{1/2}$ at each radial station.[5,6] This is shown in Fig. 7 at midannulus, $\sigma=0.9$, for both cases. The agreement is rather good, considering the number of collocation points used. A similar comparison made for the free-vortex design with the original collocation points exhibited a negative leading edge peak[17,18]; it is encouraging to see from Fig. 7 that moving the first point upstream to $x=-0.80$ effectively removes it.

On the whole, we now feel that the agreement exhibited between the two theories is as good as can be expected, given the limitations of the comparisons: viz., only graphical, rather than tabulated, values of the camber line slopes were available, and Okurounmu and McCune kept fewer terms in their radial mode series than were used here (cf. Ref. 5, Table IV). This numerical agreement supports the validity of both theories, and further complements the analytical equivalence between them, which is demonstrated in Ref. 13.

To confirm that the shift in axial collocation points was necessitated only by the high solidity in these two cases, cases 1 and 4 were rerun with the revised locations. The predicted values of c_{ps} and the sectional load distributions changed by 1% or less for case 4, and by 0.2% or less in case 1. This is felt to be within the numerical accuracy of the solutions.

V. Summary and Conclusions

A method has been presented for computing the steady loading on a three-dimensional annular blade row in linearized compressible flow, given the blade camber line. A kernel-function procedure is used to solve the integral equation relating the unknown loading to the camber line slope. The greatest advantage of the solution procedure presented here is that it allows analytical expressions to be derived for both the spanwise and chordwise integrals that are required. It also allows the various aerodynamic and performance parameters of the rotor to be expressed as simple algebraic functions of the loading expansion coefficients.

Two-dimensional strip theory is found to give adequate agreement with the sectional loading predicted by the present analysis only near midannulus. For a high hub/tip ratio, low solidity rotor it is further demonstrated that the present analysis predicts chordwise loading distributions at midannulus which are in excellent agreement with those of isolated thin-airfoil theory, for blades with both angle of attack and camber. However, near the hub and tip, and particularly for low hub/tip ratios, the error introduced by the use of two-dimensional strip theory is significant. This can be attributed to the induced angle of attack generated by the trailing vortex wakes, which is not accounted for in the strip theory.

Comparisons are also presented between the present theory, which pertains to the off-design problem, and another three-dimensional analysis,[5,6] for the design problem. These were carried out for two blade geometries: one designed to produce free-vortex flow, and the other to produce a linear increase in circulation from hub to tip. In the latter case it was found necessary to distribute the collocation points closer to the edges of the blades to obtain good agreement, due to the combined effects of high solidity and rapidly changing camber line slopes.

When coupled with the analogous treatment of the disturbance flowfield produced by blade thickness,[1-3,13,14] the loading analysis presented here should provide an efficient means of studying three-dimensional effects in turbomachinery rows. Some development work remains, however. In particular, a systematic study is needed of the effects of varying the position and number of collocation points, and hence the number of terms in the expansion of the unknown loading, particularly for high solidity rows. Also, the assumption of constant axial chord projection should be relaxed to allow application to a wider variety of blade geometries. It is believed that the techniques developed here could be used to good advantage in the prediction of unsteady blade loadings as well.

Acknowledgments

This work was supported by the Air Force Aero-Propulsion Laboratory of the Air Force Systems Command, Wright-Patterson AFB, Ohio, under Contract F33615-76-C-2092, under the technical direction of Marvin Stibich, AFAPL/TBC. The authors gratefully acknowledge the assistance of John Moselle in developing the computer program, and many useful discussions with Drs. J. C. Erickson Jr., G. R. Ludwig, J. P. Nenni, and W. J. Rae.

References

[1] McCune, J. E., "The Three-Dimensional Flow Field of an Axial Compressor Blade Row—Subsonic, Transonic, and Supersonic," Ph.D. Thesis, Cornell Univ., Ithaca, N.Y., 1958.

[2] McCune, J. E., "A Three-Dimensional Theory of Axial Compressor Blade Rows—Application in Subsonic and Supersonic Flows," *Journal of the Aerospace Sciences*, Vol. 25, Sept. 1958, pp. 544-560.

[3] McCune, J. E., "The Transonic Flowfield of an Axial Compressor Blade Row," *Journal of the Aerospace Sciences*, Vol. 25, Oct. 1958, pp. 616-626.

[4] Okurounmu, O. and McCune, J. E., "Three-Dimensional Vortex Theory of Axial Compressor Blade Rows at Subsonic and Transonic Speeds," *AIAA Journal*, Vol. 8, July 1970, pp. 1275-1283.

[5] Okurounmu, O. and McCune, J. E., "Transonic Lifting Surface Theory for Axial Flow Compressors," United Aircraft Research Laboratories, Hartford, Conn., Rept. K213580-1, March 1971.

[6] Okurounmu, O. and McCune, J. E., "Lifting Surface Theory of Axial Compressor Blade Rows, Part I—Subsonic Compressor," *AIAA Journal*, Vol. 12, Oct. 1974, pp. 1363-1371; "Part II—Transonic Compressor," pp. 1372-1380.

[7] McCune, J. E. and Dharwadkar, S. P., "Lifting-Line Theory for Subsonic Axial Compressor Rotors," MIT Gas Turbine Laboratory, Cambridge, Mass., Rept. 110, July 1972.

[8] Falcao, A. F. de O., "Three-Dimensional Flow Analysis in Axial Turbomachines," Ph.D. Thesis, Engineering Dept., Cambridge Univ., Aug. 1970.

[9] Namba, M., "Small Disturbance Theory of Rotating Subsonic and Transonic Cascades," 1st International Symposium on Air Breathing Engines, Marseille, France, June 1972.

[10] Namba, M., "Lifting Surface Theory for a Rotating Subsonic or Transonic Blade Row," Aeronautical Research Council, Great Britain, R&M 3740, Nov. 1972.

[11] Salaun, P., "Calculation of the Unsteady Subsonic Aerodynamic Pressures on Compressor Blades," *La Recherche Aerospatiale*, No. 1, Jan.-Feb. 1973, pp. 41-49.

[12] Salaun, P., "Unsteady Aerodynamic Pressure on an Annular Cascade in Subsonic Flow," Office National d'Etudes et de Recherches Aerospatiale Pub. 158, 1974; translated as European Space Agency Technical Translation ESA-TT-173, July 1975.

[13] Lordi, J. A. and Homicz, G. F., "Linearized Analysis of the Three-Dimensional, Compressible Flow through a Rotating Annular Blade Row," *Journal of Fluid Mechanics*, Vol. 103, Feb. 1981, pp. 413-442.

[14] Erickson, J. C. Jr., Lordi, J. A., and Rae, W. J., "On the Transonic Aerodynamics of a Compressor Blade Row," Calspan Corp., Buffalo, N.Y., AI-3003-A-1, Oct. 1971.

[15] Lordi, J. A., Homicz, G. F., and Ludwig, G. R., "Investigation of Rotating Stall Phenomena in Axial Flow Compressors, Vol. II—Investigation of Rotor-Stator Interaction Noise and Lifting Surface Theory for a Rotor," Air Force Aero-Propulsion Laboratory, AFAPL-TR-76-48, June 1976.

[16] Tyler, J. M. and Sofrin, T. G., "Axial Flow Compressor Noise Studies," *SAE Transactions*, Vol. 70, 1962, pp. 309-332.

[17] Homicz, G. F. and Lordi, J. A., "Three-Dimensional Lifting-Surface Theory for an Annular Blade Row," ASME Gas Turbine Conference, San Diego, Calif., Paper 79-GT-182, March 12-15, 1979.

[18] Homicz, G. F., Lordi, J. A., and Ludwig, G. R., "Aerodynamic and Acoustic Investigations of Axial Flow Fan and Compressor Blade Rows, Including Three-Dimensional Effects," Air Force Aero-Propulsion Laboratory, AFAPL-TR-79-2061, Aug. 1979.

[19] Pistolesi, E., "On the Calculation of Flow Past an Infinite Screen of Thin Airfoils," NACA TM 968, 1941.

[20] Woolard, H. W., "A Note on the Subsonic Compressible Flow About Airfoils in a Cascade," *Journal of the Aeronautical Sciences*, Vol. 17, No. 6, 1950, pp. 379-381.